Metal loaded nano-carbon gas sensor array for pollutant detection[1]

Syrine Behi [1], Juan Casanova-Chafer[*2], Ernesto González[2], Nadra Bohli[1], Eduard Llobet[*2] and Adnane Abdelghani[1]

[1] Carthage University, National Institute of Applied Science and Technology, Research Unit of Nanobiotechnology and Valorisation of Medicinal Phytoressources UR17ES22, Bp 676, 1080 Charguia CEDEX, Tunisia
[2] Department of Electronics Engineering, Universitat Rovira i Virgili, MINOS, 43007 Tarragona, Spain

E-mail: juan.casanova@urv.cat ; eduard.llobet@urv.cat

Abstract

Many research works report a sensitive detection of a wide variety of gas species. However, their in-lab detection is usually performed by using single gases and, therefore, selectivity often remains an unsolved issue. This paper reports a four-sensor array employing different nano-carbon sensitive layers (bare graphene, SnO_2@Graphene, WO_3@Graphene, and Au@CNTs). The different gas-sensitive films were characterised via several techniques such as FESEM, TEM, and Raman. First, an extensive study was performed to detect isolated NO_2, CO_2, and NH_3 molecules, unravelling the sensing mechanism at the operating temperatures applied. Besides, the effect of the ambient moisture was also evaluated. Afterwards, a model for target gas identification and concentration prediction was developed. Indeed, the sensor array was used in mixtures of NO_2 and CO_2 for studying the cross-sensitivity and developing a calibration model. As a result, the NO_2 detection with different background levels of CO_2 was achieved with an R^2 of 0.987 and an RMSE of about 22 ppb.

Keywords: graphene, carbon nanotubes, metal nanoparticle, gas sensing, sensor array

1. Introduction

The World Health Organization (WHO) estimates that air pollution causes about 7 million premature deaths every year. Therefore, there is an urgent need to develop sensitive and selective gas sensors for accurate and real-time monitoring of pollutant levels. Over the past two decades, carbon nanomaterials have seen an explosion of published papers discussing a wide spectrum of applications and, particularly, for gas sensing [1]. The most studied carbonaceous structures for the development of chemoresistive gas sensors are graphene, carbon nanotubes (CNT), and their derivatives [2–4].

These gas sensors based on carbon nanomaterials have been assiduously studied by many researchers due to their remarkable properties, especially the outstanding physical-chemical properties as low signal-to-noise ratio and high carrier mobility [5,6]. However, from the gas sensing point of view, an outstanding characteristic of carbon nanomaterials is probably their high surface-to-volume ratio, which makes them optimal for the adsorption and desorption of gas molecules from their environment. Besides, carbon nanomaterials can have their surface functionalized and wet chemistry routes, plasma treatments or ion irradiation, just to cite a few, which have been used for generating controlled surface defects and for grafting functional groups [7,8]. This approach allows even further surface modifications, for instance decorating them with metal or metal oxide

[1] Pr. A. Abdelghani dedicates this work to the memory of his Father, El Haj Amor ben Abdelghani, who passes away the 28th of July 2021 in Tunisia, may God grant him eternal rest.

nanoparticles. Thereby, it is possible to achieve the modulation of their electronic properties for enhancing their essential sensing performance parameters such as sensitivity, selectivity and stability.

Chemoresistive gas sensors are relatively simple, fast, and suitable for portable devices. This fact makes them the most common gas sensing configuration in inexpensive devices. It is worth noting that alternative transducing and detection platforms exist, which show higher accuracy, but these are usually more complex, expensive, bulky and require highly skilled personnel [9]. Indeed, carbon nanomaterials have shown additional advantages such as high chemical and thermal stability, leading to high signal-to-noise ratio, lightweight, and are suitable for being integrated into miniaturized devices [10]. Hence, they are promising candidates as sensing elements for developing low-cost and highly effective gas sensors. Currently, graphene and CNT have been widely used for sensing pollutants, poisonous and explosive gases [11–13].

This paper is focused on the detection of three harmful gases, i.e., nitrogen dioxide (NO_2), carbon dioxide (CO_2), and ammonia vapours (NH_3), which are related to anthropogenic pollution. Nitrogen dioxide is a volatile gas with a pungent smell that is harmful to both humans and the environment [14]. Inhaling low concentrations (<10 ppm) can cause severe health problems. Its exposure limit based on WHO (1997) recommendation is 0.5 ppm for an eight-hour time-weighted average (TWA) [15,16]. While the European Commission defined 200 $\mu g/m^3$ as the threshold limit exposition for 1-hour [17]. Regarding ammonia exposure, the permissible exposure limit (PEL) is 25 ppm for 8-hour TWA and 35 ppm for 10 minutes, as reported by the Occupational Safety and Health Administration (OSHA) [18]. While carbon dioxide is a well-known greenhouse gas that can be released into the atmosphere either by natural or anthropogenic processes [19]. CO_2 concentration in the air is rapidly increasing at an alarming rate and is causing many serious environmental threats, including global warming and climate change [20]. In addition, since CO_2 is exhaled with aerosols, hundreds of ppm reveal unsatisfactory ventilation in indoor spaces and, for instance, increase the infection risk of COVID-19 [21].

Given the fact that chemoresistive devices usually show poor selectivity (i.e., fail at discriminating and quantifying a specific molecule in a gas mixture), researchers have been prompted for seeking different strategies to overcome this drawback. Many research efforts have been conducted to improve some sensing parameters as sensitivity, but the selectivity issue has been usually overlooked in carbon nanomaterial research. In consequence, few works report the development of sensor arrays for paving the way towards solving this challenge. In addition, the detection of gas mixtures to better evaluate the cross-sensitivity experienced with carbon nanomaterial gas sensors is envisaged very seldom.

Sensor arrays in combination with mathematical and statistical methods have been used to perform target gas identification and concentration quantification [22–25]. For this purpose, many researchers have employed principal component analysis (PCA), linear regression methods such as principal component regression (PCR) or partial least squares regression (PLSR), and machine learning methods to implement gas exposure discrimination and quantification processes [23,26–28]. These methods are carried out using the sensor raw data or response vectors as the input of a PCA or by using the same data as a training set for building regression models.

In consequence, the present work develops a four-gas sensor array (bare graphene, SnO_2@Graphene, WO_3@Graphene, and Au@CNTs) for detecting different gases. Specifically, in the first step single gases were analysed for studying the interactions and sensing mechanisms with the sensitive layers. Besides, gas mixtures of NO_2 and CO_2 were analysed and a calibration model was developed using the data of both, single gas detection and mixture detection, for effectively predicting NO_2 concentration levels at the ppb level.

2. Experimental details

2.1 Sensor fabrication

The sensor array comprised four different sensors. Therefore, 3 different metal or metal oxide decoration steps were performed over the carbon nanomaterials. Specifically, the sensitive layers developed comprised bare graphene, WO_3@graphene, SnO_2@graphene, and Au@CNTs.

The graphene-based gas sensors employed in this paper were fabricated following a protocol already published [29]. Thereby, a graphene suspension was prepared by adding 10 mg of graphene nanoplatelets in 10 mL of ethanol. The graphene used was purchased from Strem Chemicals Inc. (MA, USA, under reference no. 06-0235). These graphene nanoplatelets present a significant oxygen content (about 8%) owing to oxygen vacancies and oxygenated functional groups grafted at the surface. Thereby, better dispersibility can be achieved and the surface reactivity towards gas molecules is enhanced. In addition, oxygenated species and defects are probably enhancing the immobilization of the nanoparticles in the carbon surface [30]. Afterwards, the graphene suspensions were exfoliated for one hour in an ultrasonic bath (Bandelin electronic GmbH, Germany) at a high frequency (35 kHz) to prevent the agglomeration of graphene. In parallel, another two suspensions were prepared with metal oxide nanoparticles. Specifically, 1 mg of tin oxide (SnO_2) and 2 mg of tungsten oxide (WO_3) were respectively dispersed in 10 mL of ethanol. The SnO_2 and WO_3 were commercially available nanopowders purchased from Sigma Aldrich (Saint

Louis, MO, USA). Subsequently, a final solution was prepared by decorating the graphene samples with a 5%wt of nanoparticles under vigorous stirring for 30 minutes.

Regarding the multi-walled carbon nanotubes (Nanocyl S.A., Belgium), they also were functionalized with oxygen functional groups and vacancies via a plasma treatment [31]. As mentioned before, the presence of functional groups on the outer wall of CNTs improves their surface reactivity [32,33]. Once the deposition of CNT on the sensor substrate was carried out, they were then decorated with gold nanoparticles (Au) by the sputtering technique. The sputtering parameters were regulated to 30 W under argon plasma for 20 s at a pressure of 0.1 Torr.

These four types of sensors that employed carbon nanomaterials were deposited on commercial alumina substrates (Ceram Tech GmBH, Germany). The upper side contains interdigitated platinum electrodes with a 300 μm gap, while the bottom side presents an 8 Ω heating element for controlling the operating temperature.

2.2 Materials characterisation

The carbon nanomaterials obtained were characterised using several techniques. Transmission Electron Microscopy (TEM) was used to analyse both the morphology and the structural properties of nanomaterials. This analysis (JOEL JEM 2100F, Japan) was performed at 200 keV as operating voltage. A drop of the fourth dispersions was deposited onto a copper grid. Moreover, a copper grid of gold nanoparticles was placed during the gold sputtering deposition.

An alternative technique for morphology investigation such as Field-Effect Scanning Electron Microscope (FESEM) was used (Carl Zeiss AG, Oberkochen, Germany). The crystallinity of the as developed nanomaterials was evaluated using Raman Spectroscopy (Renishaw, UK), which is a reliable, sensitive, and non-destructive tool [34]. The Raman spectrometer used was coupled to a confocal Leica DM2500 microscope (Leica Microsystems GmbH, Germany). This analysis was performed by exciting the samples with a 514 nm wavelength laser.

2.3 Gas sensing setup

The developed sensors based on graphene, SnO_2@graphene, WO_3@graphene, and Au@CNT were tested for the detection of three different gas species: carbon dioxide (CO_2), nitrogen dioxide (NO_2), and ammonia vapours (NH_3).

The sensor resistance was monitored under exposure to different concentrations of these gases. Specifically, two gas channels were employed, one for synthetic air (purity 99.995%) used as a carrier gas, and the other one connected to calibrated gas bottles that contained a given pollutant balanced in dry air. An automated mass flow control system was used to generate reproducible concentrations, and it was connected to a sensor chamber (40 mL in volume) able to accommodate up to four sensors simultaneously. The overall flow was regulated at 100 mL/min and perpendicular to the sensitive layers. The chamber was designed and 3D printed to house the 4-element sensor array. Nylon Strong polyamide 6 (PA6) was used as a printing material, and the AutoCAD software from Autodesk was used for designing the chamber. In consequence, the sensors were placed close to each other in a compact way and with small dead volume (see Figure S1 in the supporting information).

Sensors were exposed for 1 hour to dry synthetic air to stabilise their baseline, followed by 30 minutes of exposure to the different target gases. The resistance changes were measured via an Agilent HP 34972A multimeter. The sensor response was defined as the normalized resistance variation expressed by the following equation:

$$\Delta R/R_0(\%) = [(R_g - R_0) \setminus R_0] \times 100$$

Where R_g is the sensor resistance measured in the presence of gas and R_0 is the sensor resistance under the carrier gas.

3. Results and discussion

3.1 Material Characterisation

The morphology, crystallinity, and distribution of metal oxide nanoparticles in the carbonaceous nanostructures were assessed through several techniques.

3.1.1 FESEM characterisation

Figure 1 shows the images obtained by FESEM for the four sensors developed. Figure 1(a) shows an image of bare graphene with high porosity that makes them a good candidate for gas sensors by increasing the potential interaction with gas molecules owing to a larger surface area. Specifically, the BET (Brunauer-Emmett-Teller) area, and the pore size and volume for graphene nanoplatelets were analysed in previous experiments [35]. First, graphene was degassed overnight at 120 ºC and subsequently the nitrogen adsorption-desorption analysis was conducted, resulting in a BET area of about 730 m²/g using the BJH (Barret, Joyner, and Halenda) method. In addition, an average pore diameter of 1.73 nm and a pore volume of 1.04 cm3/g were obtained. These parameters lead to efficient adsorption and desorption of gas molecules.

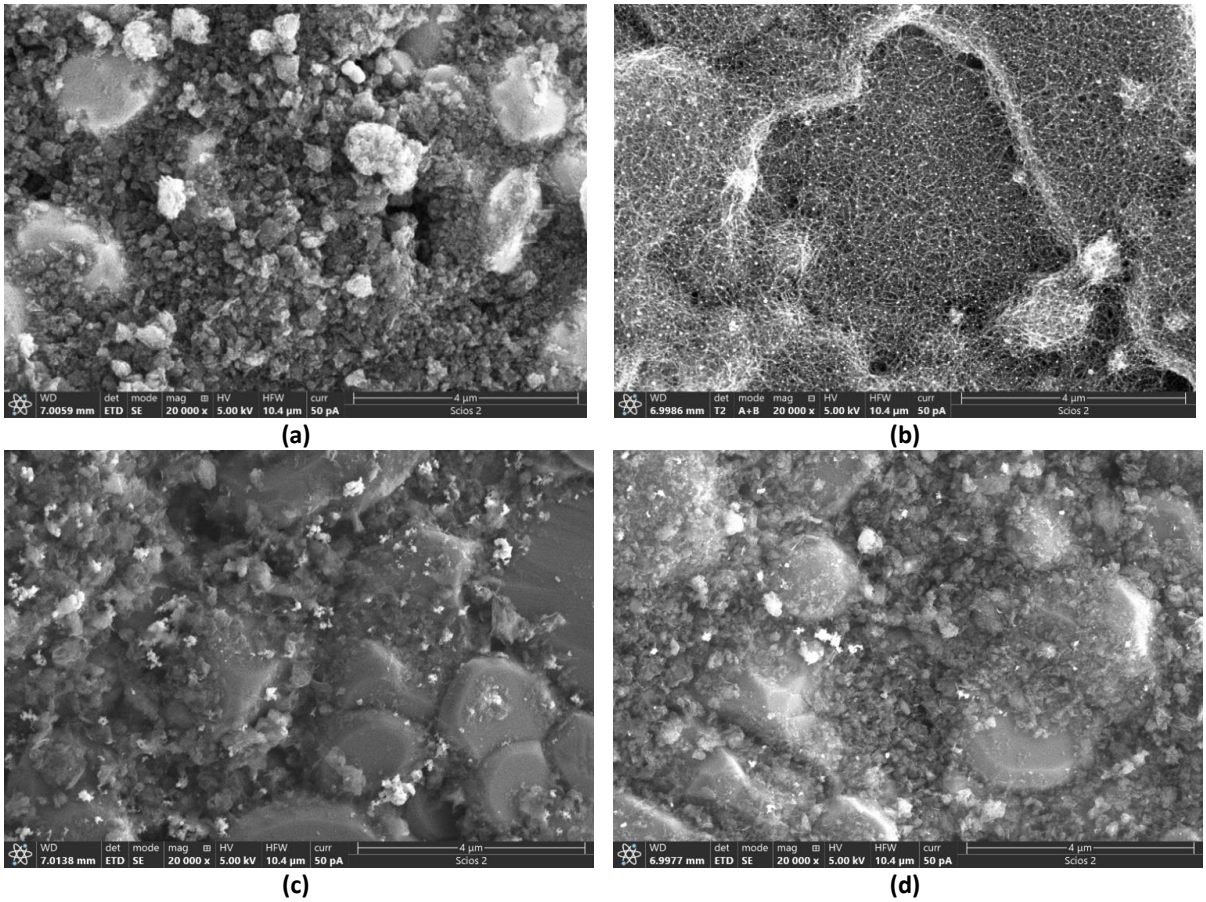

Figure 1. FESEM images showing the morphology of the different samples studied (a) bare graphene, (b) Au@MWCNTs, (c) SnO_2@Graphene, (d) WO_3@Graphene.

The surface topography of carbon nanotubes and graphene decorated with nanoparticles is observed in Figure 1(b-d). It can be observed a suitable uniformity of the sensitive films. However, additional FESEM images were obtained using a Back-Scattered Electron Detector (BSD) for revealing the nanoparticle distribution (Figure S2). Bright dots indicate the presence of metallic nanoparticles attached to the surface of CNTs and graphene, while the dark background represents the graphene nanoplatelets.

Overall, these FESEM images highlight that the distribution of WO_3 and SnO_2 on the graphene surface and gold nanoparticles on CNTs are quite homogeneous. However, Au NPs revealed a better distribution than WO_3 and SnO_2, owing to the deposition method. In this perspective, gold sputtering leads to a more homogeneous distribution than stirring and ultrasonic processes. Conversely, sputtering deposition requires more expensive and complex facilities.

It is worth noting that sometimes the nanoparticles are agglomerated, denoting that further optimizations can be performed. Nevertheless, SnO_2 and WO_3 nanoparticles with relatively uniform size are anchored to a large number of graphene nanoplatelets.

In addition, the graphene used contains a significant amount of oxygen functional groups (7.8% wt.[36]) derived from their protocol synthesis followed. These oxygen groups can easily interact with the metal oxide nanoparticles, thus improving the decoration of graphene and immobilizing the nanoparticles.

3.1.2 TEM characterisation

TEM analysis was also conducted for all the sensors developed. Figure 2(a) shows that graphene sheets consist of a few thin and transparent layers. The dark fields observed correspond to the stacked layers on top of each other with fewer folds and creases [37]. The diameter of graphene sheets is less than 2 microns, and the thickness is about a few nanometers.

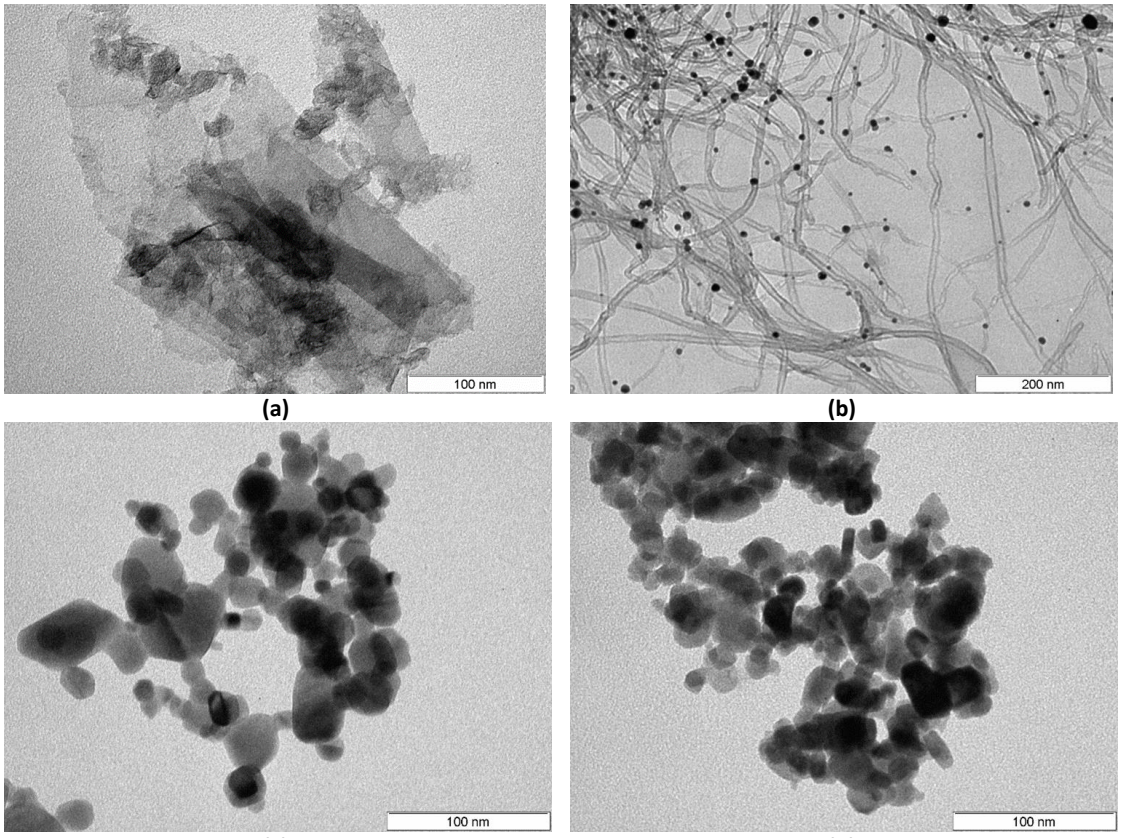

Figure 2. TEM images showing the morphology of the different samples studied (a) bare graphene, (b) Au@MWCNTs, (c) SnO_2 NPs, (d) WO_3 NPs.

Figure 2(b) shows the TEM micrograph of Au@CNTs. The gold nanoparticles are successfully grafted onto the sidewalls of the CNTs which are approximately 50 µm in length and their inner and outer diameters are close to 3 and 15 nm, respectively. Besides, a copper grid of gold nanoparticles deposited by sputtering technique was also used, revealing an average size of Au nanoparticles of about 3.7±1.4 nm (Figure 3). Figures 2(c) and 2(d) show the nanoparticle size for tin oxide and tungsten oxide nanoparticles, respectively. These images reveal an average size of about 24.4 ± 8.0 nm and 20.7 ± 2.4 nm for SnO_2 and WO_3, respectively. Figure S3 depicts different histograms summarizing the nanoparticle size distributions.

3.1.3 Raman characterisation

The crystallinity was evaluated by using Raman spectroscopy (Figure 4). It can be observed the well-known D band at 1310 cm^{-1}, the G band at 1590 cm^{-1}, and the 2D band at 2620 cm^{-1}. The D and 2D bands represent the defects and disorder surface structures (e.g., carbonaceous impurities, amorphous carbon, or broken sp^2 bonds) [38,39]. Conversely, the G band is related to the in-plane vibrations of sp^2 bonded carbon atoms [40]. An estimation of the number of graphene layers can be obtained considering the intensity ratio I_{2D}/I_G. As expected, Figure 4 shows an I_{2D}/I_G ratio lower than 1, revealing a multilayer graphene [41].

Combining the intensities of the D and G bands (I_D/I_G ratio) the crystallinity of carbon nanomaterials can be also assessed owing to evaluate the abundance of defects on the structures [42]. Experimentally, the value of the I_D/I_G ratio of bare graphene is 1.67 and for decorated graphene is 1.59. While the ratio for Au@CNTs is 1.56. These negligible differences indicate that the decoration processes followed do not damage the carbon structures. Nevertheless, the relatively high values obtained even for bare graphene reveal a low level of crystallinity in origin, but the presence of defects and impurities can be beneficial for the interaction with gas molecules. Conversely, desorption of the gas molecules can

be challenging, especially when the gas sensors are operated at room temperature. However, increasing the operating temperatures up to 200ºC is usually enough to promote the gas desorption from the sensor surface and recover the original resistance values.

3.2 Sensing results

Even though carbon-based sensors can operate at room temperature to detect gases, bare graphene configurations usually lead to poor sensing performance. Some alternatives, as the anchoring of organic molecules to the graphene surface, improve the sensing performance in ambient conditions [43]. However, some drawbacks as poor reversibility should be overcome. Another option is the graphene decoration with metal or metal oxide nanoparticles, which usually enhance several sensing parameters like sensitivity and detection limits. The inclusion of metal oxide nanoparticles, which may exhibit catalytic properties over room temperature [44], prompted us to investigate the performance of these hybrid nanomaterials at moderate temperatures (up to 250°C). Therefore, the different sensors produced were tested for NO_2, CO_2, and NH_3 detection at different operating temperatures (room temperature, 150, 200, and 250 °C). It was found that 200°C is the optimal temperature for NO_2 and CO_2 detection in terms of highest response and stability, whereas for detecting NH_3 the best operating temperature was established at 150°C. The results on the performance of sensors as a function of the operating temperature can be found in the supplementary information (see Figure S4-6).

For a matter of clarity, all sections below only present the response and recovery curves for the WO_3@Graphene sensor.

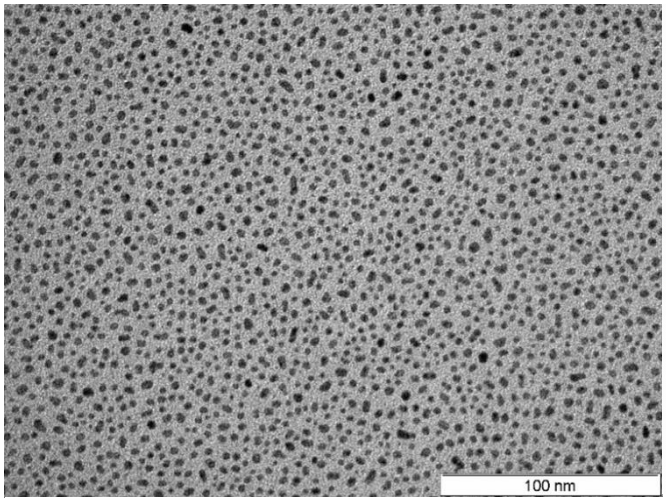

Figure 4. TEM micrograph of gold nanoparticles obtained by plasma sputtering.

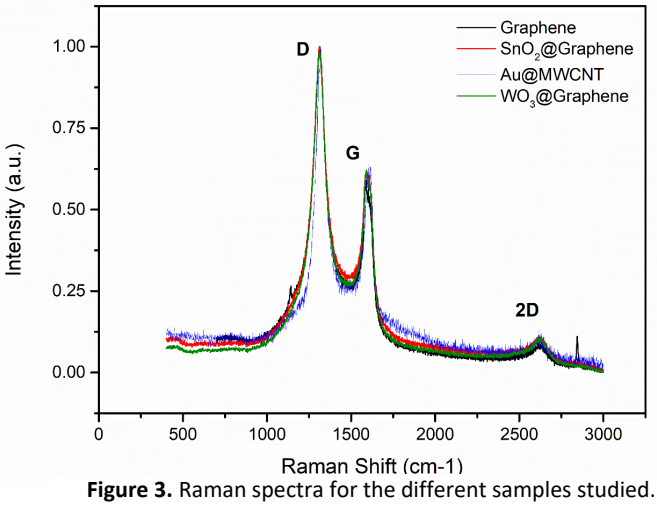

Figure 3. Raman spectra for the different samples studied.

Nevertheless, all responses of the other sensors produced are summarized in the supporting information.

3.2.3 NO_2 detection

An example of the dynamic sensing responses to NO_2 is presented in Figure 5(a). Specifically, low concentrations were applied [45] (250, 500, 750, and 1000 ppb). The lowest concentration detected was 250 ppb and their corresponding resistance change was about ~9% for graphene-based gas sensors, revealing high sensing responses for detecting NO_2 (Figure S7).

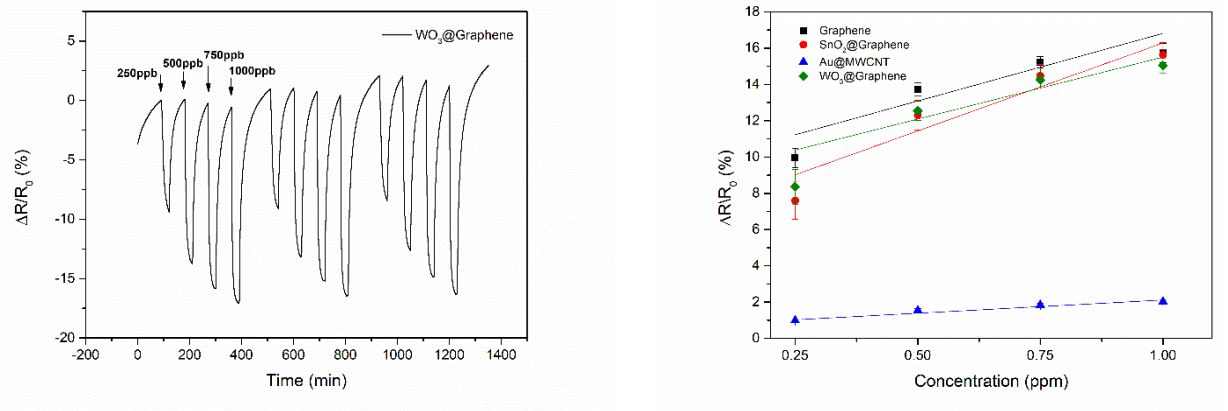

Figure 5. (a) Example of dynamic response of Graphene+WO_3 sensor for detecting NO_2 at 200°C. (b) Calibration curves obtained for NO_2 of different sensors studied.

Conversely, as Figure 5(b) revealed, the responses for the Au@CNT sensor were significantly lower. Indeed, the sensitivity for NO_2 was determined based on the slope of the calibration curves, which are summarized in Table S1. Overall, the graphene-based sensors have a sensitivity ~5 times higher to NO_2 than the Au@CNT sensor.

As expected, increasing NO_2 concentrations lead to higher resistance changes. Besides, it is well-known that NO_2 molecules act as electrons acceptors, hence the interaction with sensitive layers that behave as p-type semiconductors [46,47] leads to a decrease in their resistance.

It is worth noting that when operating above room temperature, atmospheric oxygen has a significant role in the sensing mechanisms since it can interact with the sensitive layers as follows:

NO_2 molecules can directly interact with the sensor surface, extracting electrons from the conduction band as shown in Eq. (1). However, atmospheric oxygen also has a significant role when operating above room temperature. Therefore, additional mechanisms as the interaction of NO_2 with the chemisorbed oxygen species (O^- and O^-_2) cannot be ruled out [48].

$$\boldsymbol{NO_{2(gas)} + e^- \rightarrow NO^-_{2(ads)}} \quad (1)$$

Roughly, these multiple interactions probably enhance the sensing responses for all the sensors tested, leading to greater resistance changes when exposed to NO_2. In addition, it is well-known that NO_2 molecules present a larger charge transfer than other gases as NH_3 or H_2, to cite some [49]. In consequence, significant and fast sensing responses were obtained. It is worth noting that the operating temperature applied enables the sensitization of the surface, enhancing the sensing performance. Besides, the different nanomaterials showed a suitable sensor recovery when exposed to pure dry air, denoting that 200ºC are enough for an effective desorption of NO_2 molecules. As a result, the original resistance baseline level was achieved after the gas exposure most of the times.

3.2.4 CO_2 detection

The process used to detect CO_2 was similar to that used for NO_2. But in this case, four concentrations were analysed at ppm range (25, 50, 75, and 100 ppm Figure 6(a) shows the real-time response curve to CO_2 at 200°C when using the WO_3@Graphene sensor (the other dynamic responses are summarized in the supporting information Figure S8). The sensor resistance increases when exposed to CO_2 owing to their behaviour as electron donor molecules. In consequence, the hole concentration decreases and, given the fact that holes are the majority carriers in p-type semiconductors, this results in reduced conductivity.

Figure 6(b) shows the calibration curves obtained for the different sensors employed. When exposed to 100 ppm the highest sensor response was around 5%. This fact reveals lower charge transfers than those registered for NO_2. Nevertheless, higher CO_2 concentrations (i.e., sensor saturation) or long exposures may compromise the fully recovering of the resistance baseline, requiring additional approaches to correct the baseline drift. At 200 ºC, the target gas probably interacts with layered oxygen ions (O^{-2}), resulting in the formation of carbonate ions as given in Eq. 2 [50].

$$\boldsymbol{CO_{2(gas)} + O^{-2}_{(ads)} \rightarrow CO^{-2}_{(ads)}} \quad (2)$$

3.2.5 NH_3 detection

Figure 7(a) shows the response and recovery curves of four concentrations (25, 50, 75, and 100 ppm) of ammonia at 150°C (the other responses are in Figure S9). It can be observed a slight baseline drift, probably because ammonia interacts with higher energy binding than other gas species as NO_2 [51]. Thereby, the recovery process under dry airflow is not enough to effectively desorb and clean the sensor surface.

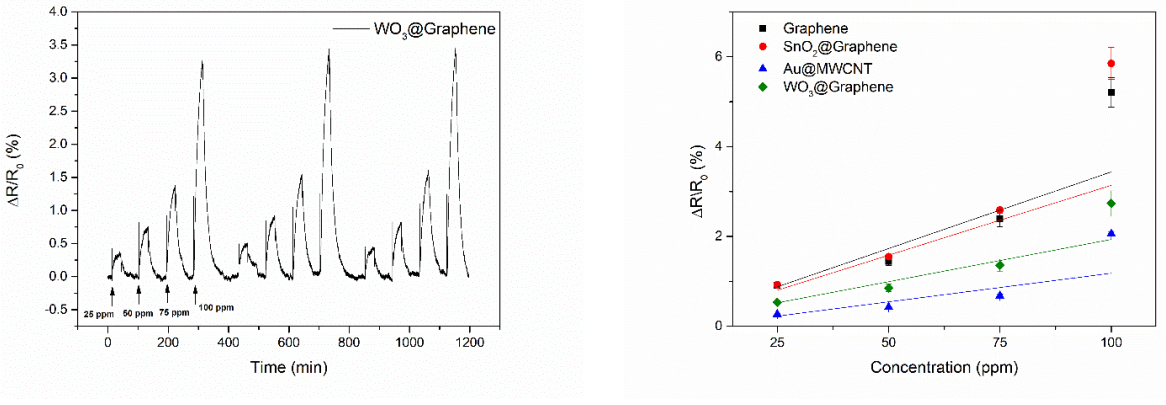

Figure 6. (a) Example of dynamic response of Graphene+WO_3 sensor for detecting CO_2 at 200°C. A linear baseline correction was implemented to ameliorate the resistance drift over time caused by the partial desorption of CO_2 molecules. (b) Calibration curves obtained for CO_2 of different sensors studied.

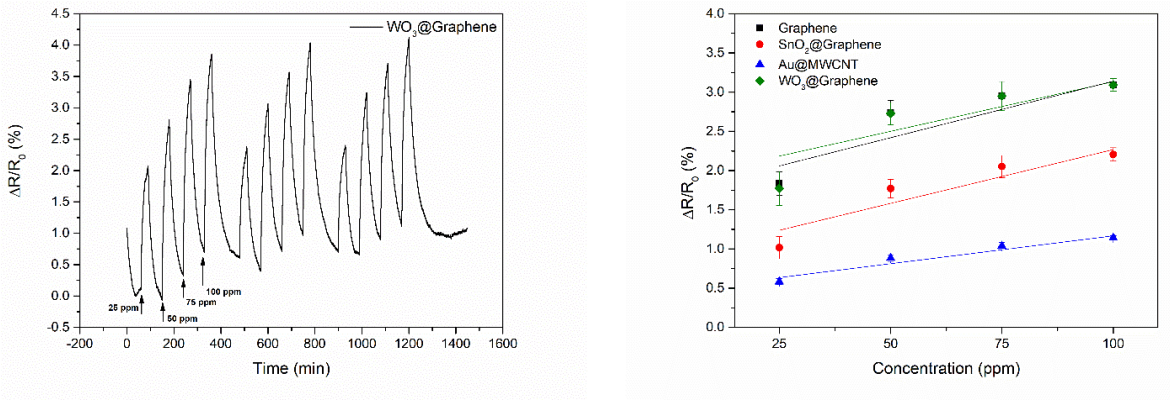

Figure 7. (a) Example of dynamic response of Graphene+WO_3 sensor for NH_3 at 150°C. (b) Calibration curves obtained for NH_3 of different sensors studied.

It is worth noting that until 150 ºC, NH_3 was acting as electron donor, while from 200 ºC this gas was acting as electron-withdrawing. In other words, at temperatures below 150 ºC the resistance increases while well above 200 ºC the sensor resistance decreases (Figure S10). This phenomenon can be explained by the predominance of different sensing mechanisms. At low temperatures, NH_3 molecules were probably reacting with oxygen species according to Eq. 3. Besides, considering the measurements in dry air, the continuous oxygen contribution can create a complementary doping effect. In other words, when NH_3 molecules directly interact with graphene, there is an electron transfer from the gas compound to the carbon nanomaterial. Then, the oxygen already adsorbed on the sensor surface coming from the atmosphere and the H_2O generated as a subproduct of Eq. 3 can improve the electron extraction from graphene. Thereby, oxygen and H_2O act as electron acceptors, inducing an additional charge transfer. As a result, the graphene Fermi level is further shifted upward [52], releasing a higher number of positive carriers that would be available to interact with NH_3, enhancing the sensing response. Conversely, at higher temperatures the release of a strong oxidizing subproduct as NO_x in the presence of oxygen species (Eq. 4) can explain this change in the behaviour [53,54]:

$$\boldsymbol{2NH_3 + 3O^- \rightarrow N_2 + 3H_2O + 3e^-} \qquad (3)$$

$$\boldsymbol{4NH_3 + 5O_2^- \rightarrow 4NO + 6H_2O + 5e^-} \qquad (4)$$

3.3 Humidity test

The effect of humidity on gas sensing performance was also evaluated (Figure S11). Indeed, the same experimental conditions as NO_2 detection at 200°C and in dry conditions were applied again, but in this case, the atmosphere was humidified with a 50% relative humidity [2,55]. Thereby, the sensors were exposed to different concentrations (250, 500, 750, 1000 ppb) as shown in Figure 8(a). The dynamic responses to varying NO_2 concentrations were similar to those obtained in dry conditions, meaning good reproducibility and resistance baseline stability. However, calibration curves represented in Figure 8(b) reveal higher resistance changes for the four sensitive layers when are operated in humid conditions. The reason is that H_2O molecules act as an electron-withdrawing like NO_2 gas [56]. In consequence, their simultaneous presence creates an additive effect, increasing the sensing responses obtained. Specifically, at 200ºC, the water molecules probably undergo dissociative adsorption as given in Eq. 5 [57]:

$$H_2O_{(gas)} \rightarrow OH^- + H^+ \quad (5)$$

Interestingly, despite the higher responses obtained in the presence of ambient moisture, the sensor sensitivity, given by the slope of the calibration curves, was slightly reduced in comparison to dry conditions. The reason is probably the change in the baseline resistance level (~5 times reduced) since H_2O was applied during both phases, exposure and recovery. This fact can mask, to some extent, the resistance change induced by the exposure to NO_2 owing to the additive effect mentioned before.

3.4 Target gas identification and concentration quantification

Considering the previous gas sensing results, the limit of detection (LOD) of each sensor was calculated for the different gases tested. This value was estimated as *LOD = 3Sa/b*, where *Sa* corresponds to the standard deviation of y-intercepts, while *b* is the slope of the calibration curve. Table 1 summarizes the detection limits experimentally obtained. It is worth noting that comparable results were obtained for the different compositions of the sensitive films.

Table 1. Limits of detection obtained for the different gases employing the four carbon-based compositions.

Sensor	NO_2 (ppb)	CO_2 (ppm)	NH_3 (ppm)
Graphene	136.1	16.3	21.4
Au@MWCNT	59.8	16.9	9.7
WO_3@Graphene	190.4	11.4	25.5
SnO_2@Graphene	127.3	32.9	14.9

Besides, once the sensor responses towards different concentrations of CO_2, NO_2, and NH_3 were evaluated at different temperatures, the obtained values at their respective optimal temperatures were used to build linear regression models. These models were employed to predict the target gases

concentrations employing the developed sensor array. First, loadings and scores from the PCA (obtained using data from the four synthesized sensors) were employed for creating a biplot. This result was used for selecting the sensors to be employed in the linear regression models. For sensor exposures to CO_2 (Figure S12a) and NO_2 (Figure S12b), the different concentrations are organized in a separated cluster according to the 1st PC axis. In both cases, the SnO_2@Graphene sensor loading presents the highest projection on the 1st PC axis, and its orientation is relatively orthogonal to the Au@CNT sensor loading. Thus, SnO_2@Graphene and Au@CNT sensor responses were used to build the linear regression models. Figure 9 shows the PLSR calibration model and cross-validation results obtained for the sensor exposure to (a) NO_2 and (b) CO_2 concentrations at 200 ºC when the SnO_2@Graphene and Au@CNTs sensor responses were used to build the training matrix. The results obtained show R^2 values of about 0.93 and RMSE values of about 10 % of the concentration range measured.

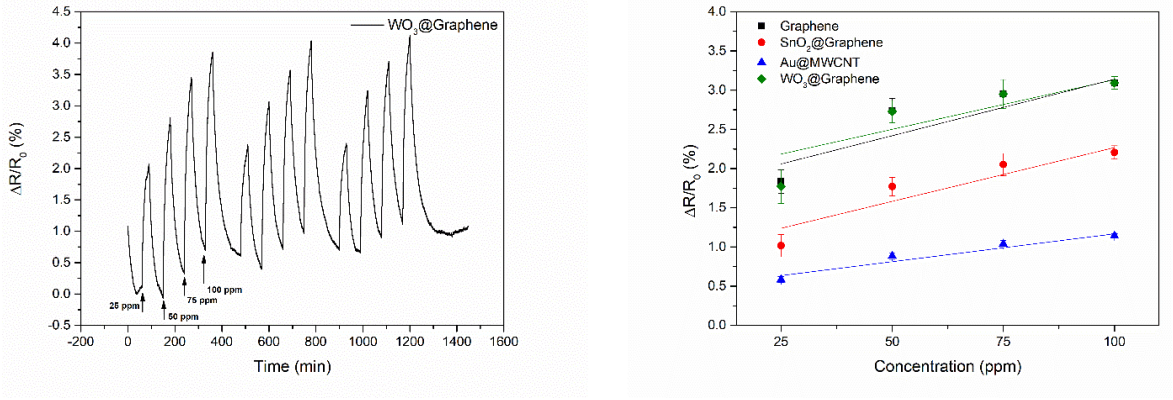

(a) **(b)**

Figure 8. (a) Example of dynamic response of Graphene+WO_3 sensor for NH_3 at 150°C. (b) Calibration curves obtained for NH_3 of different sensors studied.

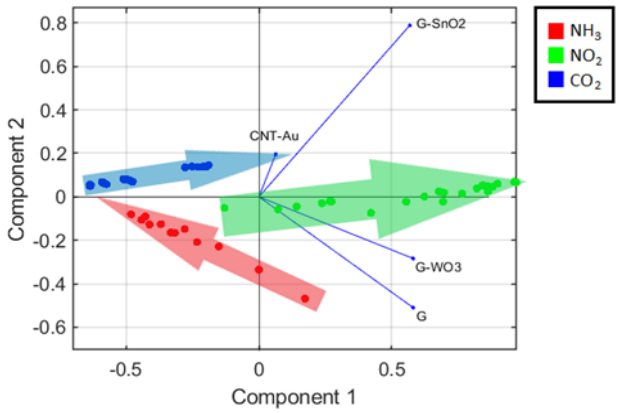

Figure 10. PCA loadings and scores biplot developed using the four sensors' response toward single gas exposition to build the matrix. Arrows' directions depict the direction of increasing concentrations.

Regarding the NH_3 responses, the PCA scores do not show a clear separation between the different concentrations tested (Figure S12c). Experimental observations are relatively oriented according to the 2nd PC, although these are overlapped in a unique cluster, suggesting that the application of linear regression models will not lead to obtaining good concentration prediction performance. Indeed, results from the PLSR model for predicting ammonia concentrations show an R^2 value lower than 0.80 and an RMSE higher than 17 % of the measured concentration range in the best of cases, using three sensors to build the training matrix. Hence, the foreseen poor performance of the sensor array for predicting NH_3 concentrations was confirmed.

After analysing the performance towards each gas separately, a PCA biplot was built using the four sensor responses towards each of the three studied gases as a unique matrix to analyse the possibility of identifying the different gases using sensor responses. Figure 10 shows the PCA loadings and scores biplot obtained when the response from the four sensors towards the three studied gases are used to build the training matrix. Scores from the PC1 and PC2 are represented in the biplot since these components gather more than 99% of the model variance. In this sense, the scores obtained from increasing concentrations of every single gas are aligned in a well-defined direction, allowing the identification of the specific gas by separating the observations from each gas in different clusters. However, at high concentrations of NH_3, their scores can be close to the scores belonging to the low CO_2 concentrations.

3.5 Cross-sensitivity test

Since the CO_2 and NO_2 scores observations followed parallel directions, these two gases were selected to perform a cross-sensitivity test. For this purpose, the sensors were exposed to consecutive cycles of 200 and 600 ppb of NO_2 with different background concentrations of CO_2 (10 and 60 ppm). The dynamic sensing responses are shown in supporting information (Figure S13 and S14). It is worth noting that stable and reproducible responses were obtained in gas mixtures. In addition, Figure 11 depicts the PLSR calibration model and cross-validation results for this cross-sensitivity test. Figure 11(a) shows the results obtained by considering the gas mixtures only. In other words, validation results are shown for variable NO_2 concentrations under a background concentration of 10, and 60 ppm of CO_2, measurements corresponding to single NO_2 exposures are not included. As a result, the PLSR shows an R^2 value of 0.9879 and an RMSE value of about 3 % of the measured NO_2 concentration range. Conversely, Figure 11(b) shows the validation results when the measurements corresponding to single exposures to NO_2 were also considered, i.e., the background concentrations of CO_2 were (0, 10, and 60 ppm of CO_2). The calibration model shows an R^2 value of 0.8834 and an RMSE value of about 12% for the measured NO_2 concentration range.

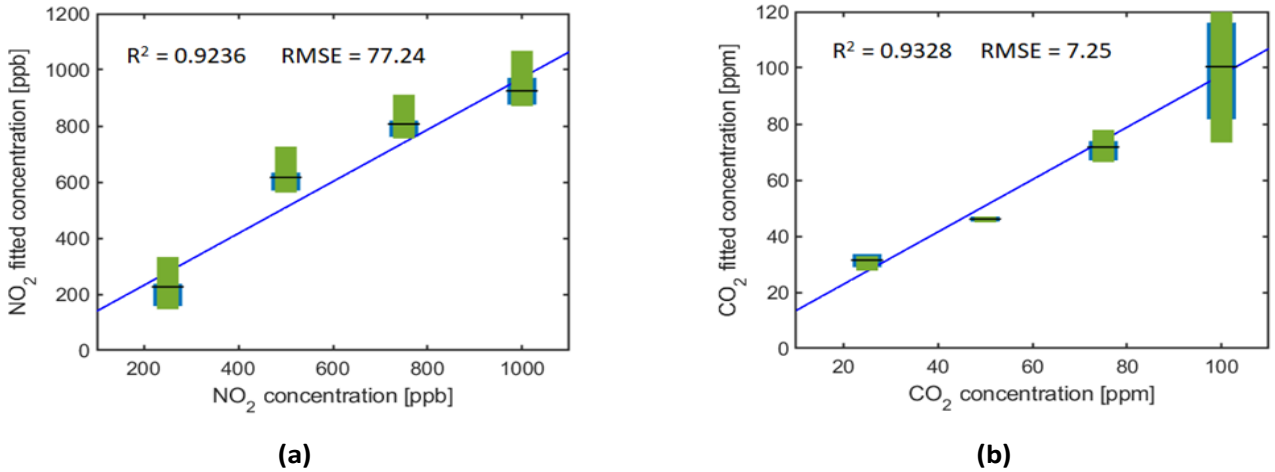

Figure 9. PLSR calibration model and validation for (a) NO_2 and (b) CO_2 concentrations using the SnO_2@Graphene and Au@MWCNTs sensors response at 200 ºC to build the training matrix.

Interestingly, better results were obtained using a mixture of gases, in which NO_2 is the target gas and a background level of CO_2 was included as an interfering species. Thereby, since different compositions show overlapping responses to several gases, it is not feasible achieving a significant selectivity enhancement using a single sensor. In consequence, to overcome the existing cross-sensitivity, the use of sensor arrays and the combination of the data (cross data) is needed to create a training matrix able to discriminate the target gases from interfering compounds. This result can pave the way towards the development and optimization of sensor arrays for predicting pollutant levels under operating conditions closer to those needed in real applications.

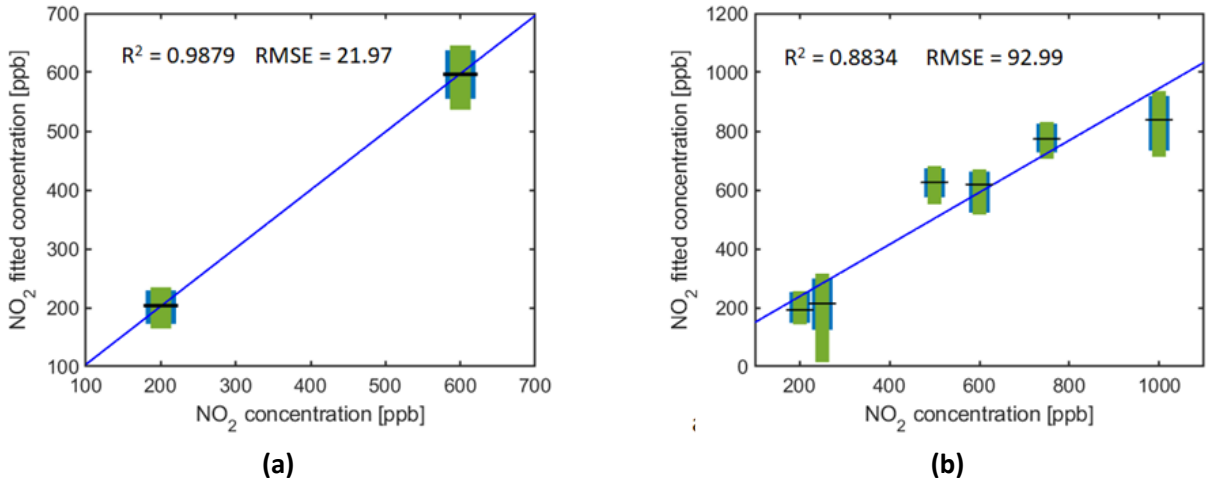

Figure 11.PLSR calibration model and cross-validation performed using the sensor responses towards (a) just NO_2 in presence of two different background concentrations of CO_2, (b) isolated NO_2 concentrations, and NO_2 in presence of two different background concentrations of CO_2.

4. Conclusions

A gas sensor array comprising four carbon-based nanomaterials decorated with metal or metal oxides was implemented. The array was exposed to three different pollutant species and its reponse was studied.

The application of a principal component ananlysis to the responses of the sensor for the three polluttant species considered revealed that SnO_2@Graphene and Au@CNTs sensors present a relatively orthogonal behaviour. Thus, these sensors were selected for building regression models aimed at predicting pollutant concentrations. Indeed, different NO_2 target concentrations were detected under several backgrounds levels of CO_2 as an interfering species. As a result, R^2 values of about 0.987 and RMSE of 22 ppb were achieved, demonstrating the high potential of the developed approach to estimate the concentration of a target pollutant in mixtures.

Nevertheless, further optimizations should be done by fine-tuning the nanomaterials employed and the amount of gases tested. In addition, further cross-sensitivity studies are needed before its implementation in real applications.

Acknowledgements

Pr.A. Abdelghani thanks the Alexander von Humboldt Foundation (Bonn, Germany) for the material donation and the Science for Peace and Security Program of the North Atlantic Treaty Organization (SPS-NATO, grant G5571) for the funding. E.L. is supported by the Catalan Institution for Research and Advanced Studies via the 2018 Edition of the ICREA –Academia Award.

References

[1] Umadevi D and Sastry G N 2014 Feasibility of carbon nanomaterials as gas sensors: A computational study *Curr. Sci.* **106** 1224

[2] Shaik M, Rao V, Gupta M, Murthy K and Jain R 2016 Chemiresistive gas sensor for the sensitive detection of nitrogen dioxide based on nitrogen doped graphene nanosheets *RSC Adv.* **6** 1527–34

[3] Casanova-Cháfer J, Bittencourt C and Llobet E 2019 Hydrophilicity and carbon chain length effects on the gas sensing properties of chemoresistive, self-assembled monolayer carbon nanotube sensors *Beilstein J. Nanotechnol.* **10** 565–77

[4] Tang X, Debliquy M, Lahem D, Yan Y and Raskin J-P 2021 A Review on Functionalized Graphene Sensors for Detection of Ammonia *Sensors* **21** 1443

[5] Llobet E 2013 Gas sensors using carbon nanomaterials: A review *Sens. Actuators B Chem.* **179** 32–45

[6] Kim M I and Lee Y-S 2016 A comprehensive review of gas sensors using carbon materials *J. Nanosci. Nanotechnol.* **16** 4310–9

[7] Travlou N A, Seredych M, Rodríguez-Castellón E and Bandosz T J 2015 Activated carbon-based gas sensors: effects of surface features on the sensing mechanism *J. Mater. Chem. A* **3** 3821–31

[8] Lonkar S P, Deshmukh Y S and Abdala A A 2015 Recent advances in chemical modifications of graphene *Nano Res.* **8** 1039–74

[9] Bielecki Z, Stacewicz T, Smulko J and Wojtas J 2020 Ammonia Gas Sensors: Comparison of Solid-State and Optical Methods *Appl. Sci.* **10** 5111

[10] Liang G, Xiaolin M, Guiyun T, Qi H, Junaid A and Ze H 2019 Current Applications of Gas Sensor Based on 2-D Nanomaterial: A Mini Review | Chemistry

[11] Misra A 2014 Carbon nanotubes and graphene-based chemical sensors *Curr. Sci.* **107** 419–29

[12] Wang T, Huang D, Yang Z, Xu S, He G, Li X, Hu N, Yin G, He D and Zhang L 2016 A Review on Graphene-Based Gas/Vapor Sensors with Unique Properties and Potential Applications *Nano-Micro Lett.* **8** 95–119

[13] Gupta Chatterjee S, Chatterjee S, Ray A K and Chakraborty A K 2015 Graphene–metal oxide nanohybrids for toxic gas sensor: A review *Sens. Actuators B Chem.* **221** 1170–81

[14] Elsayed N M 1994 Toxicity of nitrogen dioxide: an introduction *Toxicology* **89** 161–74

[15] Lee S W, Lee W, Hong Y, Lee G and Yoon D S 2018 Recent advances in carbon material-based NO2 gas sensors *Sens. Actuators B Chem.* **255** 1788–804

[16] 2014 Recommendation from the Scientific Committee on Occupational Exposure Limits for Nitrogen Dioxide. Available online: https://ec.europa.eu/social/BlobServlet?docId=12431&langId=en (Accessed on 7 July 2021)

[17] Standards - Air Quality - Environment - European Commission. Available online: https://ec.europa.eu/environment/air/quality/standards.htm. (Accessed on 13 January 2022)

[18] Bannov A G, Popov M V, Brester A E and Kurmashov P B 2021 Recent Advances in Ammonia Gas Sensors Based on Carbon Nanomaterials *Micromachines* **12** 186

[19] Yoon H J, Jun D H, Yang J H, Zhou Z, Yang S S and Cheng M M-C 2011 Carbon dioxide gas sensor using a graphene sheet *Sens. Actuators B Chem.* **157** 310–3

[20] Lin Y and Fan Z 2020 Compositing strategies to enhance the performance of chemiresistive CO2 gas sensors *Mater. Sci. Semicond. Process.* **107** 104820

[21] Virbulis J, Sjomkane M, Surovovs M and Jakovics A 2021 Numerical Model for Prediction of Indoor COVID-19 Infection Risk Based on Sensor Data *J. Phys. Conf. Ser.* **2069** 012189

[22] Palacín J, Martínez D, Clotet E, Pallejà T, Burgués J, Fonollosa J, Pardo A and Marco S 2019 Application of an Array of Metal-Oxide Semiconductor Gas Sensors in an Assistant Personal Robot for Early Gas Leak Detection *Sensors* **19** 1957

[23] Szulczyński B, Namieśnik J and Gębicki J 2017 Determination of Odour Interactions of Three-Component Gas Mixtures Using an Electronic Nose *Sensors* **17** 2380

[24] Deng F, Chen W, Wang J and Wei Z 2018 Fabrication of a sensor array based on quartz crystal microbalance and the application in egg shelf life evaluation *Sens. Actuators B Chem.* **265** 394–402

[25] Gongwei X, Chutian Y, Weigen C, Lingfeng J and Sirui T 2017 Study on the development and test method of SnO2-based gas sensor array for dissolved gas analysis *2017 13th IEEE International Conference on Electronic Measurement Instruments (ICEMI)* 2017 13th IEEE International Conference on Electronic Measurement Instruments (ICEMI) pp 220–7

[26] Sett A, Rana T, Roy R, Saha T and Bhattacharyya T K 2020 Selective detection of multiple VOCs employing zinc oxide nanorods and principle component *2020 4th International Conference on Electronics, Materials Engineering Nano-Technology (IEMENTech)* 2020 4th International Conference on Electronics, Materials Engineering Nano-Technology (IEMENTech) pp 1–6

[27] Skotadis E, Kanaris A, Aslanidis E, Michalis P, Kalatzis N, Chatzipapadopoulos F, Marianos N and Tsoukalas D 2020 A sensing approach for automated and real-time pesticide detection in the scope of smart-farming *Comput. Electron. Agric.* **178** 105759

[28] Burgués J and Marco S 2018 Multivariate estimation of the limit of detection by orthogonal partial least squares in temperature-modulated MOX sensors *Anal. Chim. Acta* **1019** 49–64

[29] Behi S, Bohli N, Casanova-Cháfer J, Llobet E and Abdelghani A 2020 Metal Oxide Nanoparticle-Decorated Few Layer Graphene Nanoflake Chemoresistors for the Detection of Aromatic Volatile Organic Compounds *Sensors* **20** 3413

[30] Charlier J-C, Arnaud L, Avilov I V, Delgado M, Demoisson F, Espinosa E H, Ewels C P, Felten A, Guillot J, Ionescu R, Leghrib R, Llobet E, Mansour A, Migeon H-N, Pireaux J-J, Reniers F, Suarez-Martinez I, Watson G E and Zanolli Z 2009 Carbon nanotubes randomly decorated with gold clusters: from nano2hybrid atomic structures to gas sensing prototypes *Nanotechnology* **20** 375501

[31] Hafaiedh I, Clément P, Baccar H, Llobet E and Abdelghani A 2013 Functionalised multi–walled carbon nanotubes for chemical vapour detection *Int. J. Nanotechnol.* **10** 485–95

[32] Thamri A, Baccar H, Struzzi C, Bittencourt C, Abdelghani A and Llobet E 2016 MHDA-Functionalized Multiwall Carbon Nanotubes for detecting non-aromatic VOCs *Sci. Rep.* **6** 35130

[33] Baccar H, Thamri A, Clément P, Llobet E and Abdelghani A 2015 Pt-and Pd-decorated MWCNTs for vapour and gas detection at room temperature *Beilstein J. Nanotechnol.* **6** 919–27

[34] Hao Y, Wang Y, Wang L, Ni Z, Wang Z, Wang R, Koo C K, Shen Z and Thong J T L 2010 Probing Layer Number and Stacking Order of Few-Layer Graphene by Raman Spectroscopy *Small* **6** 195–200

[35] Casanova-Chafer J, Umek P, Acosta S, Bittencourt C and Llobet E 2021 Graphene Loading with Polypyrrole Nanoparticles for Trace-Level Detection of Ammonia at Room Temperature *ACS Appl. Mater. Interfaces* **13** 40909–21

[36] Casanova-Cháfer J, García-Aboal R, Atienzar P and Llobet E 2019 Gas sensing properties of perovskite decorated graphene at room temperature *Sensors* **19** 4563

[37] Meyer J C, Geim A K, Katsnelson M I, Novoselov K S, Booth T J and Roth S 2007 The structure of suspended graphene sheets *Nature* **446** 60–3

[38] Casanova-Cháfer J, Navarrete E, Noirfalise X, Umek P, Bittencourt C and Llobet E 2019 Gas Sensing with Iridium Oxide Nanoparticle Decorated Carbon Nanotubes *Sensors* **19** 113

[39] González E, Casanova-Chafer J, Romero A, Vilanova X, Mitrovics J and Llobet E 2020 LoRa Sensor Network Development for Air Quality Monitoring or Detecting Gas Leakage Events *Sensors* **20** 6225

[40] Jorio A 2012 Raman spectroscopy in graphene-based systems: prototypes for nanoscience and nanometrology *Int. Sch. Res. Not.* **2012**

[41] Nguyen V T, Le H D, Nguyen V C, Ngo T T T, Le D Q, Nguyen X N and Phan N M 2013 Synthesis of multi-layer graphene films on copper tape by atmospheric pressure chemical vapor deposition method *Adv. Nat. Sci. Nanosci. Nanotechnol.* **4** 035012

[42] Wu J-B, Lin M-L, Cong X, Liu H-N and Tan P-H 2018 Raman spectroscopy of graphene-based materials and its applications in related devices *Chem. Soc. Rev.* **47** 1822–73

[43] Tang X, Mager N, Vanhorenbeke B, Hermans S and Raskin J-P 2016 Defect-free functionalized graphene sensor for formaldehyde detection *Nanotechnology* **28** 055501

[44] Cho B, Yoon J, Hahm M G, Kim D-H, Kim A R, Kahng Y H, Park S-W, Lee Y-J, Park S-G, Kwon J-D, Kim C S, Song M, Jeong Y, Nam K-S and Ko H C 2014 Graphene-based gas sensor: metal decoration effect and application to a flexible device *J. Mater. Chem. C* **2** 5280–5

[45] Brunet J, Garcia V P, Pauly A, Varenne C and Lauron B 2008 An optimised gas sensor microsystem for accurate and real-time measurement of nitrogen dioxide at ppb level *Sens. Actuators B Chem.* **134** 632–9

[46] Yuan W and Shi G 2013 Graphene-based gas sensors *J. Mater. Chem. A* **1** 10078

[47] Zanolli Z, Leghrib R, Felten A, Pireaux J-J, Llobet E and Charlier J-C 2011 Gas Sensing with Au-Decorated Carbon Nanotubes *ACS Nano* **5** 4592–9

[48] Ghimbeu C M, Schoonman J, Lumbreras M and Siadat M 2007 Electrostatic spray deposited zinc oxide films for gas sensor applications *Appl. Surf. Sci.* **253** 7483–9

[49] Mehdi Aghaei S, Monshi M M, Torres I, Zeidi S M J and Calizo I 2018 DFT study of adsorption behavior of NO, CO, NO2, and NH3 molecules on graphene-like BC3: A search for highly sensitive molecular sensor *Appl. Surf. Sci.* **427** 326–33

[50] Arshak K and Gaidan I 2005 Development of a novel gas sensor based on oxide thick films *Mater. Sci. Eng. B* **118** 44–9

[51] Travan C and Bergmann A 2019 NO2 and NH3 Sensing Characteristics of Inkjet Printing Graphene Gas Sensors *Sensors* **19** 3379

[52] Cao G, Liu X, Liu W, Li Q, Li X and Wang X 2017 Chemical environment dominated Fermi level pinning of a graphene gas sensor *Carbon* **124** 57–63

[53] Gautam M and Jayatissa A H 2012 Ammonia gas sensing behavior of graphene surface decorated with gold nanoparticles *Solid-State Electron.* **78** 159–65

[54] Khun Khun K, Mahajan A and Bedi R 2009 SnO2 thick films for room temperature gas sensing applications *J. Appl. Phys.* **106** 124509

[55] Sasaki I, Minami N, Karthigeyan A and Iakoubovskii K 2009 Optimization and evaluation of networked single-wall carbon nanotubes as a NO2 gas sensing material *Analyst* **134** 325–30

[56] Deokar G, Casanova-Cháfer J, Rajput N S, Aubry C, Llobet E, Jouiad M and Costa P M F J 2020 Wafer-scale few-layer graphene growth on Cu/Ni films for gas sensing applications *Sens. Actuators B Chem.* **305** 127458

[57] Wang C, Yin L, Zhang L, Xiang D and Gao R 2010 Metal Oxide Gas Sensors: Sensitivity and Influencing Factors *Sensors* **10** 2088–106